ELSEVIER

Chemical Engineering Journal 71 (1998) 221–231

Chemical Engineering Journal

A numerical analysis of NO_x formation and control in radiatively/conductively-stabilized pulverized coal combustors

Changsik Kim, Noam Lior*

Department of Mechanical Engineering and Applied Mechanics, University of Pennsylvania, 297 Towne Bldg/220, S0.33rd St., Philadelphia, PA 19104-6315, USA

Received 23 July 1997; accepted 9 June 1998

Abstract

In an attempt to study ways for reducing NO_x emissions from radiatively/conductively-stabilized combustors (RCSC) for pulverized coal, a comprehensive conjugate heat and mass transfer and reaction kinetics model of that combustor was developed. As compared with a much simpler three-reaction model, the radiation intensity distribution obtained by the new model shows a substantial decrease in the flame region. The analysis has shown that (1) the effect of a 10% deviation in the diffusion coefficients on the results was found to be negligible, indicating that the use of binary coefficients instead of those for a multi-component system may be good enough in such combustion modeling, (2) flame location was found to have little effect (~6%), and internal wall emittance an insignificant effect, on NO emissions, (3) the mass fraction of these emissions could be lowered by lowering the flame temperature, accomplished by increasing the excess air ratio, (4) at the same time, the overall mass of NO emitted with the thicker lower-temperature flames produced by such increases in excess air was much higher, indicating that the RCSC with its capability for producing a high temperature thin flame is much more effective for the reduction of NO emissions than lower temperature combustion alternatives.

Keywords: Radiatively; Conductively; Stabilized combustors

1. Introduction

The primary objective of this research is to study, and explore ways to reduce, the formation and emissions of NO_x in the radiatively/conductively stabilized combustor (RCSC) for pulverized coal, which was shown in the past to reduce NO_x emissions by up to two orders of magnitude when used with fluid fuels.

As known well, NO_x is produced through the oxidation of the molecular nitrogen in combustion air and the organically bound nitrogen in the coal (thermal and fuel NO_x, respectively). Generally, 60–80% of the total NO_x produced from coal combustion is fuel NO_x [1]. Although NO_x can be formed from molecular nitrogen and hydrocarbon fragments resulting from the devolatilization process near the reaction zone of flame ('prompt NO'), it is insignificant in coal combustion (typically accounts for less than 5% of the total NO formed; [2]) and usually neglected in modeling. While the temperature sensitive thermal NO_x mechanism is well understood, the temperature insensitive fuel NO_x mechanism has been more difficult to understand due to the complex process involving both homogeneous and heterogeneous reactions.

In most combustion devices the energy necessary to heat the fuel to the point of ignition is supplied by back-mixing either by molecular or turbulent diffusion. The back-mixing produces an extended reaction zone, contact between the fuel–air mixture and the products of combustion, and oscillations. These three side-effects are known to enhance NO_x formation. A method for stabilizing combustion by radiation and conduction was explored analytically and experimentally by Churchill, Lior and co-workers for many years (cf. [3–7]) with gases, volatile oil and propane/pulverized–coal mixture fuels (the latter mixture was studied only in the pre-ignition zone). In the studies using *fluid fuels*, they have demonstrated that extremely low levels of NO_x (5–100 ppm) were generated (a reduction of about an order of magnitude as compared with conventional burners), mostly because of the rapid heating of the fuel and minimal back-mixing of the products of combustion in such burners.

Further studies are being conducted to examine its effect on the emissions of NO_x and other pollutants when used to burn *pulverized coal*. To that end, we have developed a comprehensive numerical conjugate heat transfer model of the combustor interior and walls, combining radiation, convection, and conduction [8] and validated it experimentally. The spectral radiative properties of the medium, a

*Corresponding author.

1385-8947/98/$ – see front matter
PII: S1385-8947(98)00113-2

mixture of combustion gas and particles, was also taken into account in the model. Simplified reaction kinetics were used. This model was significantly improved in the current study to include the mass transfer equations for the participating gas species and a comprehensive kinetic model, including 13 chemical species, so that the emission characteristics, such as NO_x production and destruction, during coal combustion in such a combustor could be estimated.

2. Modeling of radiatively/conductively-stabilized combustion

2.1. Combustor and process description

In this method of radiatively/conductively-stabilized combustion, depicted in Fig. 1, the thermal feedback occurs by radiation from the hot downstream region of the burner to the colder upstream region and also by longitudinal conduction through the tube wall in the same direction. The cold, unburned gases entering the tube are heated to the ignition temperature primarily by convection from the tube wall (but also by convection from the radiantly-heated particles when solid fuels are used). The hot, burned gases, in turn, heat the downstream wall by convection.

A schematic diagram of the combustor is shown in Fig. 2. The incoming gas and particles are preheated by convection from the combustor wall and by radiation from the flame

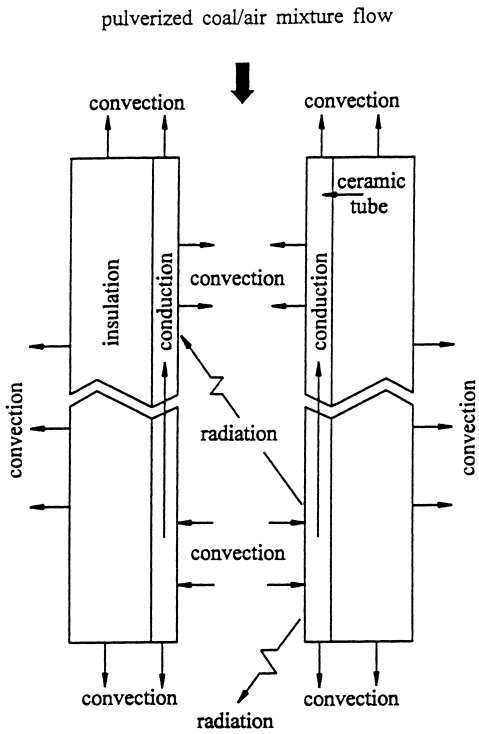

Fig. 1. The thermal feedback mechanism in the radiatively/conductively-stabilized combustor.

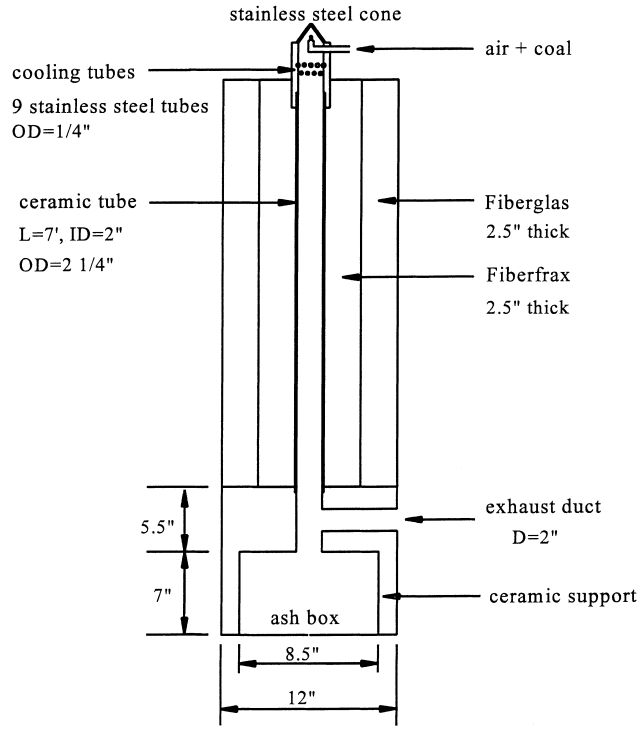

Fig. 2. The combustor (RCSC).

zone. Since the coal particles absorb more radiation than the gas, their temperature is expected to increase more rapidly. As the particles' temperature rises, they release volatile matter which then mixes with the gas stream and burns. It is generally assumed that the volatiles are consumed before the solid carbon of the particle ignites, in part because their evolution prevents oxygen from reaching the particle surface [9]. The volatiles are thus assumed to diffuse immediately and burn away from the particle surface and their combustion heat raises the gas temperature. The heat is then convected to the particle. As the volatiles 'shield' surrounding the coal particle disappears, oxygen molecules reach the particle surface and the particle carbon is oxidized to carbon monoxide. Since char combustion is a slower process than devolatilization, the gas temperature increases more slowly during the solid carbon combustion phase of the process.

The basic model and the assumptions leading to its equations were described by the authors in an earlier paper [8], and thus only a brief description is presented below.

2.2. The heat transfer and flow model

The energy equations for the gas flow and the solid zone of the combustor that is composed of the ceramic tube wall and insulation are

$$\rho_g C_g u \frac{\partial T_g}{\partial z} = \frac{1}{r}\frac{\partial}{\partial r}\left[r(k_g + \rho_g C_g \varepsilon_H)\frac{\partial T_g}{\partial r}\right] + q''' - \nabla \cdot q_{rad} \quad (1)$$

$$\frac{1}{r}\frac{\partial}{\partial r}\left(r\frac{\partial T_w}{\partial r}\right)+\frac{\partial^2 T_w}{\partial z^2}=0 \tag{2}$$

The gas velocity u is determined by a conventional three-layer turbulent velocity profile.

The local heat source term q''' includes heat generated by combustion and by convection from the particles.

$$q'''=\delta_g q'''_{VM}+q'''_{CO}+N A_p h(T_p-T_g) \tag{3}$$

where δ_g (assumed as 0.5 in this study) is the fraction of the heat generated from volatile matter combustion, q'''_{VM}, that is transferred to the gas. q'''_{CO} (=9789 kJ/kg-carbon) is the heat generated from the oxidation of CO to CO_2.

The above energy equations are solved with the following boundary conditions.

$$-k_{w1}\frac{\partial T_{w1}}{\partial r}=-k_{w2}\frac{\partial T_{w2}}{\partial r} \text{ and } T_{w1}=T_{w2} \text{ at } r=R_2,\quad 0\le z\le L \tag{4}$$

$$-k_{w2}\frac{\partial T_{w2}}{\partial r}=-k_{w3}\frac{\partial T_{w3}}{\partial r} \text{ and } T_{w2}=T_{w3} \text{ at } r=R_3,\quad 0\le z\le L \tag{5}$$

$$-k_{w3}\frac{\partial T_{w3}}{\partial r}=h(T_{w3}-T_\infty) \text{ at } r=R_4,\ 0\le z\le L \tag{6}$$

$$-k_w\frac{\partial T_w}{\partial z}=\varepsilon_w\sigma T_w^4+h(T_w-T_\infty) \text{ at } z=0,L,\ R_1\le r\le R_4 \tag{7}$$

$$T_g=T_\infty \text{ at } z=0,\ 0\le r\le R_1 \tag{8}$$

$$\frac{\partial T_g}{\partial r}=0 \text{ at } r=0,\ 0\le z\le L \tag{9}$$

$$-k_w\frac{\partial T_w}{\partial r}=-k_g\frac{\partial T_g}{\partial r}+q_{rad} \text{ and } T_g=T_w \text{ at } r=R_1,\quad 0\le z\le L \tag{10}$$

2.3. The coal particle combustion model

Coal combustion consists of two different stages: (i) devolatilization and volatile matter combustion and (ii) combustion of residue carbon, i.e., char. To solve the energy equation in the gas flow, Eq. (1), the energy released from these processes must be known. In this section, devolatilization and carbon consumption rate from char which determine the amount of energy release will be described.

When a coal particle is subjected to heating, volatile gases are given off first. Then heavier organic compounds escape from the coal as the heating continues, and, finally, tars volatilize. The amount of volatile matter evolved depends on the thermal history such as heating rate, peak temperature, and duration of heating ([10–12]). Although many devolatilization models have been developed, they were not applicable to all kind of coals due to coal type-dependent kinetic parameters. According to [13], a dual-reaction model also gives acceptable results for volatile release calculation, and this is the model we have used in our previous study [8].

With the assumption of uniform particle temperature, the energy equation of a coal/char particle is formulated as

$$\frac{1}{6}d_p\rho_p C_p\frac{dT_p}{dt}=h(T_g-T_p)+\varepsilon_p(I-\sigma T_p^4)-\frac{dm_p}{dt}\Delta H+(1-\delta_g)q'''_{VM}+Kq_p P_{O_2} \tag{11}$$

This equation is coupled with the gas-phase energy equation, Eq. (1), and solved together. The particle is assumed to be solid although both coal and char particles are often porous. Due to the limited understanding of surface transport rates and kinetics, consideration of porosity would have complicated this model immensely, without clear benefits.

It is assumed in this study that carbon is oxidized initially to carbon monoxide by the reaction

$$C+\tfrac{1}{2}O_2\rightarrow CO \tag{12}$$

and further oxidized to carbon dioxide far from the particle.

For this rate limiting oxidation of carbon monoxide, the global rate expression suggested in [14] (R8 in Table 2) was used.

2.4. Radiative heat transfer

The radiative contribution to heat transfer, expressed as the divergence of the radiative flux vector in the gas energy equation (Eq. (1)) and as the intensity field in the particle energy equation (Eq. (11)), is calculated from the radiation intensity distribution in the combustor which is described by the integro-differential radiative transfer equation (RTE). By using the lowest order spherical harmonics method ($P-1$ approximation), the RTE is transformed into a partial differential equations.

$$\frac{\partial^2 I_0}{\partial \bar r^2}+\frac{1}{\bar r}\frac{\partial I_0}{\partial \bar r}+\frac{\partial^2 I_0}{\partial \bar z^2}=-3(1-\omega_0)(\omega_0 g-1)\tau_0^2(4\pi I_b-I_0) \tag{13}$$

where τ_0 ($=\beta(1-\omega f)R_1$) and ω_0 ($=(1-f)\omega/(1-f\omega)$) are the normalized optical thickness in the radial direction and single scattering albedo, respectively. Marshak's boundary condition (in [15]) is used to solve this equation:

$$I_0\pm 2(1+2\nu)I_3=4\pi I_b \quad \text{at } z=0,L \tag{14}$$

$$I_0-2(1+2\nu)I_1=4\pi I_b \quad \text{at } r=R_1 \tag{15}$$

The first moments of intensity, I_1 and I_3, are given as

$$I_1=\frac{1}{3(\omega_0 g-1)}\frac{\partial I_0}{\tau_0\partial \bar r} \tag{16}$$

$$I_3=\frac{1}{3(\omega_0 g-1)}\frac{\partial I_0}{\tau_0\partial \bar z} \tag{17}$$

The divergence of net radiative heat flux vector in the medium, needed in Eq. (1), can then be obtained from

$$\nabla\cdot q_{rad}=\int_0^\infty \kappa(4\pi I_b-I_0)d\lambda \tag{18}$$

It is important to realize that κ in Eq. (18) is the absorption coefficient of the gas only, since the energy equations for the gas and particles are considered separately. We note that the gas and particle temperatures differ up to 200–300 K in the flame region, and strictly speaking, particle emission at its temperature should have been included in the RTE. To simplify the radiative analysis somewhat, we have, however, assumed that particle emission could be considered to occur at the gas temperature, because these temperature differences are confined to the narrow flame region and as the particle size and density in such combustors is very small.

The medium inside a pulverized coal combustor is a mixture of combustion product gases and particles consisting of coal, char, fly-ash, and soot. To solve the RTE, therefore, it is necessary to take into account the spectral and temperature dependence of the radiative properties of the medium. This is especially true in a study like this, where the spatial distributions of the variables of interest are sought. All these four types of particles were considered with the assumption of uniform distribution across the tube cross-section at the inlet.

For the gas components, only carbon dioxide and water vapor are considered as major contributors to radiative heat transfer. The expression given in [16] was used for the spectral absorption coefficient (κ) of the gas components. The computationally-efficient, yet sufficiently accurate expressions proposed by the authors ([17,18]) were used to compute the spectral extinction and absorption coefficients of the coal, char, ash and soot particles. Particle size and the spectrum of radiation are imbedded in the radiative properties expressions used. The properties of the gas–particle mixture were then obtained by summation of the component contributions.

2.5. The kinetic model and NO_x formation

The kinetic mechanism for formation and destruction of NO_x involves numerous elementary reactions, making process modeling a formidable task. Simulation complexity is compounded when the flow and heat transfer phenomena are considered, as in the analysis of pulverized coal combustors. As pointed out in [19], two key aspects must, therefore, be taken into account in NO_x modeling: (i) establishment of a proper kinetic mechanism that contains sufficient detail for describing the NO_x formation/destruction process adequately, and, at the same time, (ii) limiting the number of reactions to allow for easier coupling with the much complicated heat transfer model. In agreement with condition (ii), and since the analysis of N_2O emissions requires the addition of many more kinetic and species diffusion equations, compounded by the fact that N_2O concentrations are very small in pulverized coal combustion (in the range of 0–5 ppm, [20,21]) and, therefore, also increases the complexity of the solution very significantly, our model does not yet include the reactions involving N_2O.

In this study, a global reaction model shown in Fig. 3 [22] is used to simulate volatile-NO formation and destruction, as a function of the computed temperature of the particles and the concentration. For the char-NO formation process, a kinetic mechanism suggested by the authors and their coworkers [23], depicted in Fig. 3, is used. The reactions and rate constants for the mechanisms are summarized in Tables 1 and 2, respectively. It is also assumed that half of the nitrogen in coal devolatilizes [24] and is rapidly and completely converted to HCN in the gas phase. The nitrogen remaining after devolatilization oxidizes heterogeneously to form NO at a rate equal to the rate of char weight loss. The small contribution of prompt NO to total NO is not accounted for in the analysis.

2.6. The mass diffusion model

The kinetic mechanism used in the present study includes 13 chemical species: CO, CO_2, N_2, O_2, H_2, H_2O, NO, OH, H, HCN, N, NH_3, and Ar. Considering mass diffusion in both radial and axial directions, the mass conservation

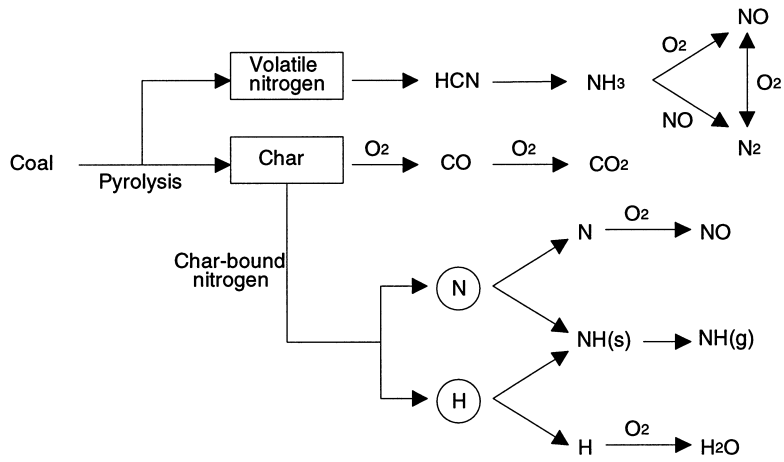

Fig. 3. The fuel NO_x formation mechanisms in the model.

Table 1
The kinetic mechanism for volatile-NO formation [22]

Reaction	Rate equation	Rate constant
(R1) N→HCN	$dN_V/dt = -k_1 N_V VM/V_\infty$	$k_1=2.63\times10^5\ \exp(-34\,000/RT)$
(R2) HCN+H_2O→NH_3+CO	$d[HCN]/dt = -k_2 y_{HCN} y_{O_2} P/R'T$	$k_2=1.94\times10^{15}\ \exp(-78\,400/RT)$
(R3) NH_3+O_2→NO+H_2O+1/2H_2	$d[NH_3]/dt = -k_3 y_{NH_3} y_{O_2}^b P/R'T$	$k_3=4.0\times10^6\ \exp(-32\,000/RT)$
(R4) NH_3+NO→N_2+H_2O+1/2H_2	$d[NH_3]/dt = -k_4 y_{NH_3} y_{NO} P/R'T$	$k_4=1.8\times10^8\ \exp(-27\,000/RT)$

Table 2
The kinetic mechanism for char-NO formation [23]

Reaction	Rate constant/rate equation
(R5) C+CO_2→2CO	$k_5=5.79\times10^{-8}\ T^{-1}\ \exp(-247.7/RT)$
(R6) C+H_2O→CO+H_2	$k_6=1.33\times10^3\ T\exp(-147.0/RT)$
(R7) C+NO→1/2N_2+CO	$k_7=3.48\times10^{20}\ \exp(-100\,000/RT)$
(R8) CO+1/2O_2→CO_2	$r_{CO}=-1.3\times10^{14}\,[H_2O]^{1/2}[CO][O_2]^{1/2}\exp(-125.5/RT)$
(R9) CO+OH→CO_2+H	$\ln k_9=10.847+3.995\times10^{-4}\ T$
(R10) CO+NO→1/2N_2+CO_2	$r_{NO}=-k_{III}P_{NO}(k_{II}P_{CO}+k_I)/k_{III}P_{NO}+k_{II}P_{CO}+k_I$
	$k_I=1.5\times10^{-3}\ \exp(-167.2/RT)$
	$k_{II}=7.33\times10^{-7}\ \exp(-79.4/RT)$
	$k_{III}=2.08\times10^{-4}\ \exp(-108.7/RT)$

equations for the species can be written as

$$\frac{\partial}{\partial z}(\rho_i u) = \frac{1}{r}\frac{\partial}{\partial r}\left[r\rho D_i \frac{\partial(\rho_i/\rho)}{\partial r}\right] + \frac{\partial}{\partial z}\left[\rho D_i \frac{\partial(\rho_i/\rho)}{\partial z}\right] + r_i, \quad i = 1, 13 \tag{19}$$

where r_i denotes the net formation rate of each component, as summarized in Table 3.

The diffusion equations are solved with the boundary conditions

$$\frac{\partial \rho_i}{\partial r} = 0 \quad \text{at } r = 0, R \tag{20}$$

While the diffusion coefficients in a binary mixture differ from those in mixtures containing more than two components, the differences are usually smaller than 10% [25]. Binary mixture coefficients were, therefore, used here. Since the oxygen here is supplied as air, about 80% of all the combustion gas is nitrogen. The binary diffusion coefficients of the different gas species are, therefore, calculated as if the only other gas present is nitrogen.

Table 3
Net formation rates of the gas components

Gas component	Formation rate
(1) CO_2	$-k_5P_{CO_2}/M_C-(r_{CO})_{R8}+k_9C_{OH}C_{CO}-(r_{NO})_{R10}$
(2) CO	$R_C/M_C-[HCN]_{R2}+2k_5P_{CO_2}/M_C+k_6C_{H_2O}+k_7C_{NO}+(r_{CO})_{R8}-k_9C_{CO}C_{OH}+(r_{NO})_{R10}$
(3) NO	$-[NH_3]_{R3}+[NH_3]_{R4}-k_7C_{NO}+(r_{NO})_{R10}$
(4) H_2O	$-[HCN]_{R2}+[NH_3]_{R4}-k_6C_{H_2O}$
(5) H_2	$1/2[NH_3]_{R3}+1/2[NH_3]_{R4}+k_6C_{H_2O}$
(6) O_2	$-1/2R_C/M_C-1/4R_H/M_H-1/2R_N/M_N-[NH_3]_{R4}+1/2(r_{CO})_{RS}$
(7) N_2	$[NH_3]_{R4}+1/2k_7C_{NO}-1/2(r_{NO})_{R10}$
(8) NH	R_{NH}/M_N
(9) H	$k_9C_{OH}C_{CO}$
(10) OH	$-k_9C_{OH}C_{CO}$
(11) HCN	$R_{HCN}/M_{HCN}+[HCN]_{R2}$
(12) NH_3	$-[HCN]_{R2}$

3. The solution method and conditions

Finite difference schemes were used to solve the governing equations, and the flow diagram of the computation logic is shown in Fig. 4. The heat transfer model developed in our previous study was augmented to include (1) the mass transfer equations for the participating gas species, and (2) a comprehensive kinetic model, including 13 chemical species, to evaluate the emissions characteristics. First a guessed temperature distribution is assigned at the interface between the gas and the tube wall. The temperature in the heated section must be high enough to produce auto-ignition of a coal particle. Based on the previous experimental results in such a combustor, an initial step temperature distribution located radially at the flow-tube interface and axially at $z=L/3$ was assigned. Then the temperature distribution in the gas flow is calculated, assuming that the gas is transparent and contains no coal particles. Thermal and physical properties of the flow are calculated as a function of temperature. Next, the coal combustion model is solved based on the gas temperature field obtained in the previous step, producing a temperature distribution of the particles and allowing the computation of the spectral radiative properties of the medium. Using the obtained properties, the RTE is solved and the radiation intensity distribution in the combustor is found. Now the heat source terms in the gas-phase energy equation, i.e., the energy released from burning coal particles q''' and the divergence of radiative heat flux q_{rad}, are known, and a new gas temperature distribution is calculated considering the energy source terms. This procedure is repeated until a converged solution is obtained for the gas temperature distribution. When acceptable convergence is achieved, the temperature distribution in the ceramic tube wall and the insulation, including that at the gas–wall interface, is calculated. Using this new temperature profile at the interface, the whole calculation procedure is repeated, and the iteration continues until a converged profile is obtained within the error limit of $O(\Delta T/T)\leq 0.1\%$.

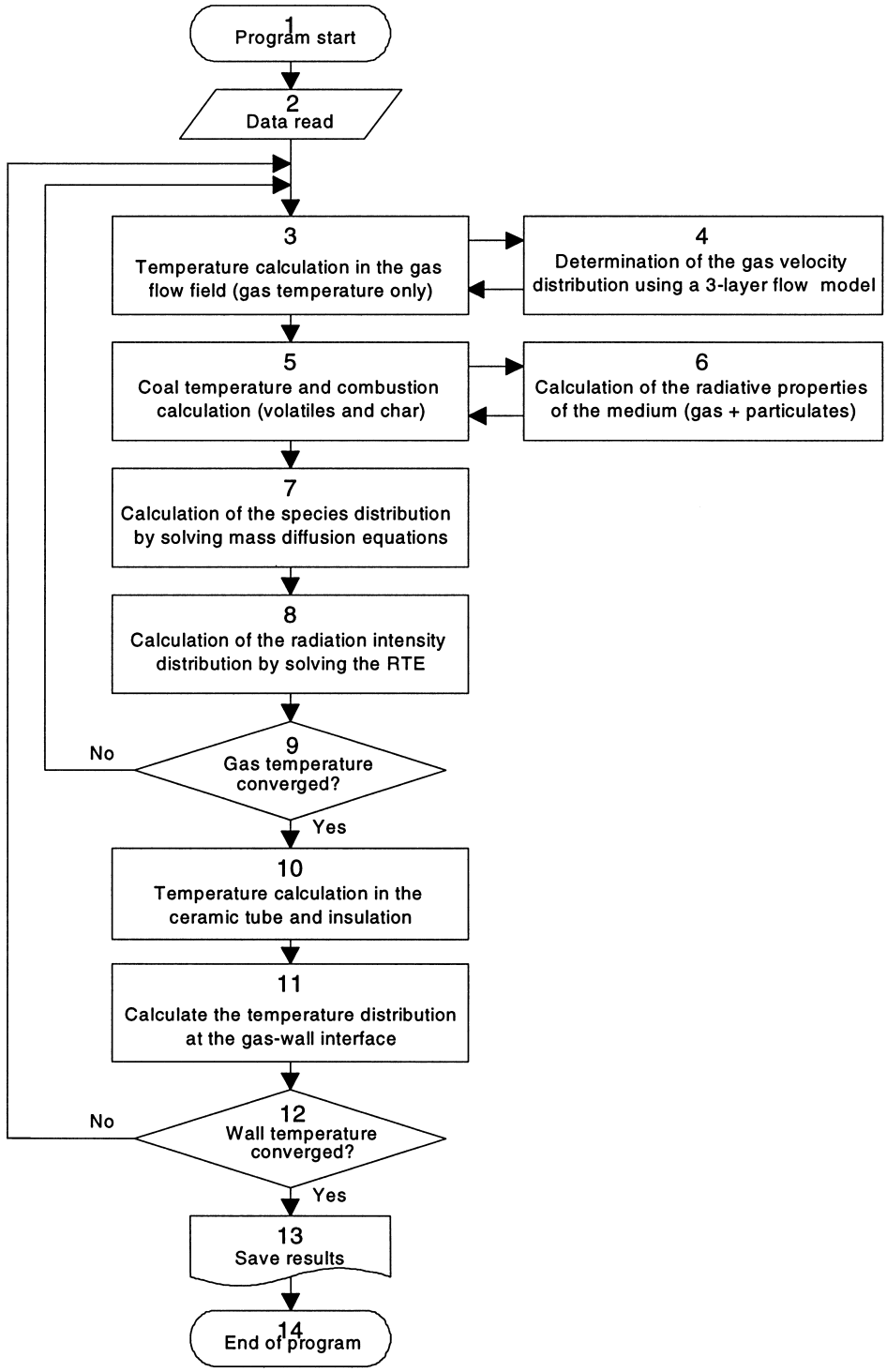

Fig. 4. The computational scheme flow diagram.

To make it most compatible with the chemical reaction kinetics in the model, low-volatiles-content, moisture-free anthracite was chosen as the coal because it has the highest C:O and C:H ratio and least amount of other elements (VM=10.8%, FC=68.6%, ash=20.6%, HHV=27732 kJ/kg). The heat of pyrolysis and the heat release from char oxidation were taken as $\Delta H=-418.6$ kJ/kg and $q_p=23281$ kJ/kg, respectively. For the computational base-case, the dimensions and properties of our experimental facility were used, with the ceramic combustor tube length $L=2.13$ m, internal diameter $2R_1=5.08$ cm, and wall thickness $t_{w1}=0.32$ cm, thermal conductivity $k_{w1}=3.61$ W/m-C, and emittance, $\varepsilon_{w1}=0.3$. The thickness of the insulation layers (Fiberfrax, t_{w2}, and Fiberglas, t_{w3}) were 6.35 cm

each and their thermal conductivities were k_{w2}=0.116 W/m-C and k_{w3}=0.0346 W/m-C, respectively. The coal feed rate is $\dot{m}=9\times10^{-5}$ kg/s, particle diameter d_p=100 μm (all of the same size, although the model can also handle size distributions), density ρ_0=1250 kg/m^3, and emittance, ε_p=0.9 for coal/char and 0.6 for ash. The diameters of ash (after the break-up of a char particle into three ash pieces) and soot particles are 30 and 0.06 μm, respectively. 100% excess air was assumed to ensure turbulent flow in the combustor. The average flow velocity at the combustor entrance was computed from the above to be 0.69 m/s.

4. Results and discussion

4.1. Effects of the kinetic model and of diffusion

To estimate the effect of the specific kinetic model and of mass diffusion on the final results, calculations were first made using a simple three-reaction kinetic model with no diffusion, and then repeated using a comprehensive kinetic model with mass diffusion. To simplify this comparative analysis, a fixed step temperature distribution along the interior surface, based on experimentally observed values typical to this combustor, was assigned as a boundary condition: T=294 K for the first 36% of the tube length and T=1255 K for the remainder (Fig. 5(a)). The comparisons between the results are shown in Figs. 5 and 6.

Fig. 5(b) shows the distribution of the Planck mean absorption coefficients of CO_2 and H_2O for both these analyzed cases. In the case of the simple kinetic model, it was assumed that carbon and hydrogen were completely converted to CO_2 and H_2O, respectively. In the comprehensive model, however, H_2O was consumed by reactions R2 and R6 (Tables 1 and 2) and the concentration decreased in the flame region. In addition, the oxidation of CO to CO_2 depends not only the concentrations of CO and O_2, but also the concentration of H_2O as can be seen from reaction R8. This could result in incomplete conversion of CO if the H_2O concentration is insufficient. The better model thus predicts lower concentrations of CO_2 and H_2O in the high-temperature zone, and consequently significantly lower values of the Planck absorption coefficient than the simpler model.

The radiative properties of the medium (a mixture of gas and particles) are shown in Fig. 5(c). When the more realistic comprehensive model was used, it was found that the extinction and absorption coefficients of the medium were significantly lower in the flame region, mostly due to the decrease of H_2O concentration. The effects of the decrease in the absorption coefficients on the distributions of temperature and radiation intensity are shown in Fig. 6. When the comprehensive kinetic model was used, the gas temperature and the radiation intensity were increased by up to 1.6% and decreased by up to 6.2%, respectively, in the flame region.

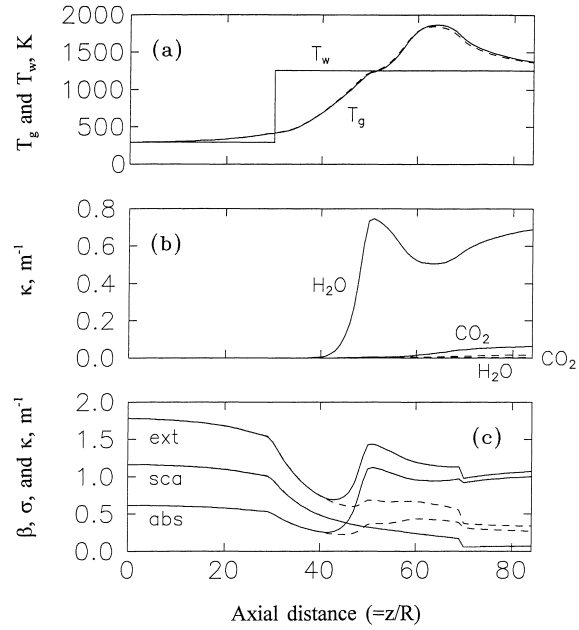

Fig. 5. Comparison of the three-reaction kinetic model (solid line) and the comprehensive kinetic model (dashed line) predictions on the axial distributions of the (a) gas and wall temperature profiles, (b) Planck mean absorption coefficient (κ) of H_2O and CO_2, (c) Planck mean extinction (ext=abs+sca), scattering (sca), and absorption (abs) coefficients, with fixed wall temperature distribution.

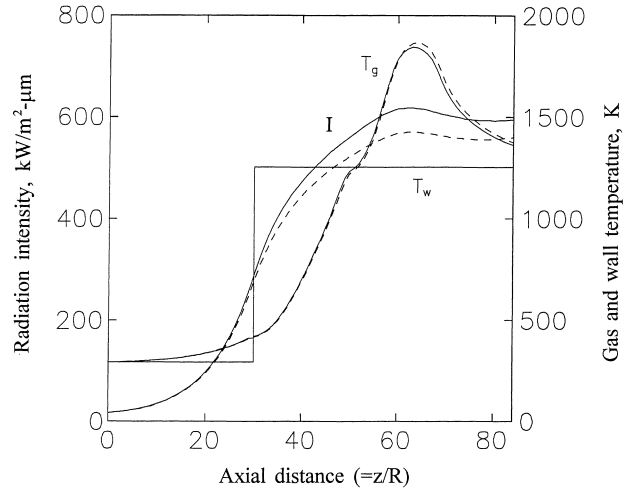

Fig. 6. Comparison of the three-reaction kinetic model (solid line) and the comprehensive kinetic model (dashed line) predictions of the radiation intensity (I) and gas temperature (T_g) distributions, with a fixed wall temperature (T_w) distribution.

We computed also the particle temperatures and have shown and discussed both gas and particle temperature distribution in a previous paper [8]. During the initial heat up, particle temperature is slightly higher than that of gas since particles absorb radiative energy from the flame and the walls. During devolatilization (which typically ends in the flame zone where the temperature rises rapidly), the gas temperature becomes higher than that of the particles, since

the volatiles burn in the gas phase. Then, when char combustion occurs, the situation reverses itself again and the particle temperature exceeds that of the gas by as much as 400 K.

Since binary, instead of multi-component, mixture diffusion coefficients were used in the analysis, it is also of interest to evaluate the effect of the uncertainties in the magnitudes of the diffusion coefficients on the results. Because binary diffusion coefficients typically differ by about 10% from those in multi-component mixtures [25], this analysis was performed by computing the temperature and radiation intensity distributions using binary diffusion coefficients varied by ±5% and ±10% from the values found from the literature [26,27].

The analysis shows that the ±5% variation in the diffusion coefficients resulted in 1.0%, 1.5%, and 0.4% change in the distribution of O_2, CO_2, and NO, respectively, and the ±10% variation resulted in a corresponding change of 2.3%, 3.0%, and 1.2%. These variations in the mass distribution do not, however, produce any noticeable change in temperature and radiation intensity distribution, indicating the use of binary diffusion coefficients is acceptable in coal combustor modeling.

Similar results were obtained when the full conjugate heat transfer problem was solved instead of pre-assigning the wall temperature distribution as described above. H_2O concentration in the flame region is found by the better kinetic model to be negligible, due to the above-described reasons, resulting also in considerable decrease in the absorption coefficient of the medium there. When the better kinetic model was used, it was found that the wall temperature increased more sharply at the flame front than when the simple model was used (Fig. 7(a)). This can be understood from the fact that approximately three-fold diminution of the extinction coefficient in the post-flame zone gas/particulates medium, predicted by the better model, allows more radiation to be absorbed in the walls. This change in radiative properties causes up to 1.9% increase in the gas temperature, while the radiation intensity decreases by 22.7% at the tube exit (Fig. 8).

4.2. Sensitivity analysis of NO_x production

Fig. 9((a) and (b)) show the distribution of the gas species considered in the comprehensive kinetic model. The concentration of carbon dioxide was found to increase in the flame downstream as the conversion of carbon monoxide progressed according to the reaction R8 which is also controlled by the concentration of H_2O. The concentration of HCN peaks in the region where devolatilization occurs as assumed and then decreases as conversion to NH_3 continues. By the two competing reactions, R3 and R4, the NH_3 subsequently produces NO and N_2 in the flame region as can be seen in Fig. 9(b). The NO_x concentration was found to peak at about 700 ppm at the axial location where the temperature peaked, and was reduced gradually towards the

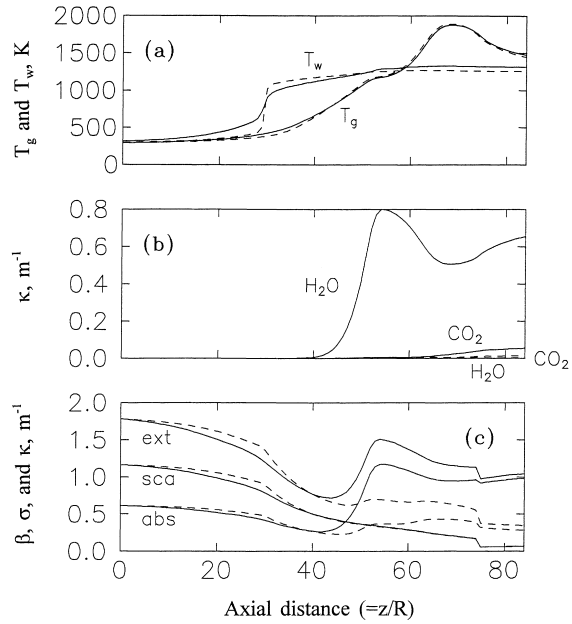

Fig. 7. Comparison of the three-reaction kinetic model (solid line) and the comprehensive kinetic model (dashed line) predictions of the axial distributions of the, (a) gas and wall temperature profiles, (b) Planck mean absorption coefficient (κ) of H_2O and CO_2, (c) Planck mean extinction (ext=abs+sca), scattering (sca), and absorption (abs) coefficients, without fixing the wall temperature distribution.

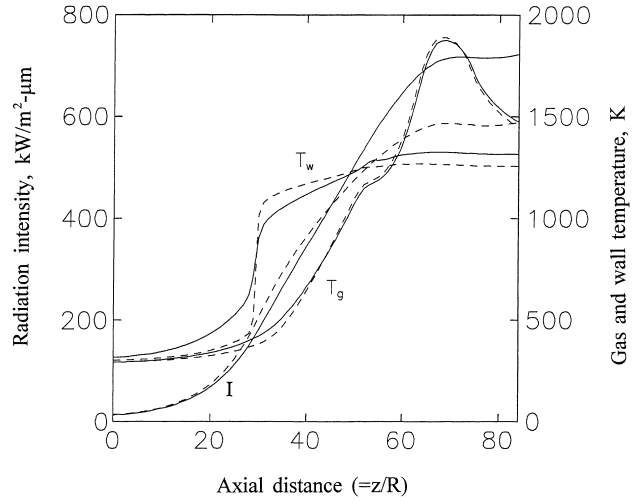

Fig. 8. Comparison of the three-reaction kinetic model (solid line) and the comprehensive kinetic model (dashed line) predictions of the radiation intensity (I), and wall temperature (T_w) and gas temperature (T_g) distributions (without fixing the wall temperature distribution).

combustor exit, primarily due to destruction by the NH_3 which was formed in the combustor.

To explore ways for reducing overall NO_x emissions, a sensitivity analysis of the effects of flame location, wall emittance, and flame thickness on NO_x emissions was conducted. The flame location was controlled by changing the position of the temperature step increase in the combustor; e.g., z=15 indicates that T=294 K for z<15 and

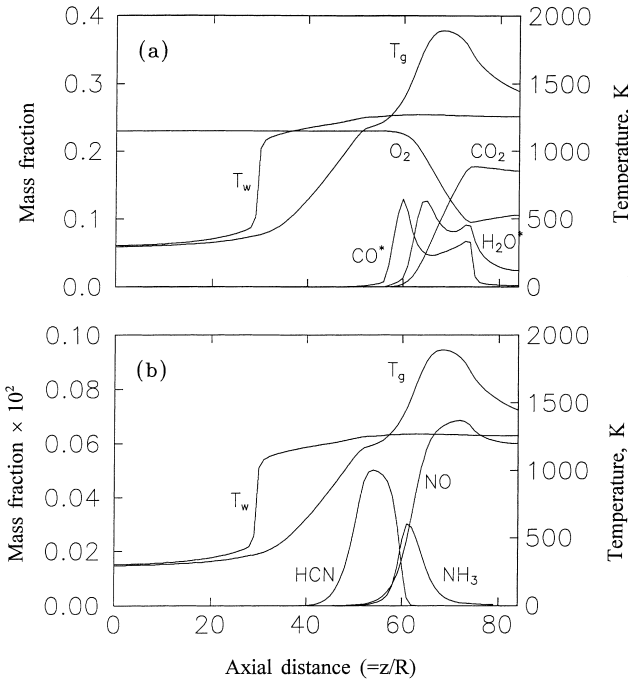

Fig. 9. The axial distribution of the wall temperature (T_w) and gas temperature (T_g) and of the mass fractions of the chemical species considered (*: mass fraction×100). (a) O_2, CO, CO_2, and H_2O, (b) HCN, NH_3, and NO.

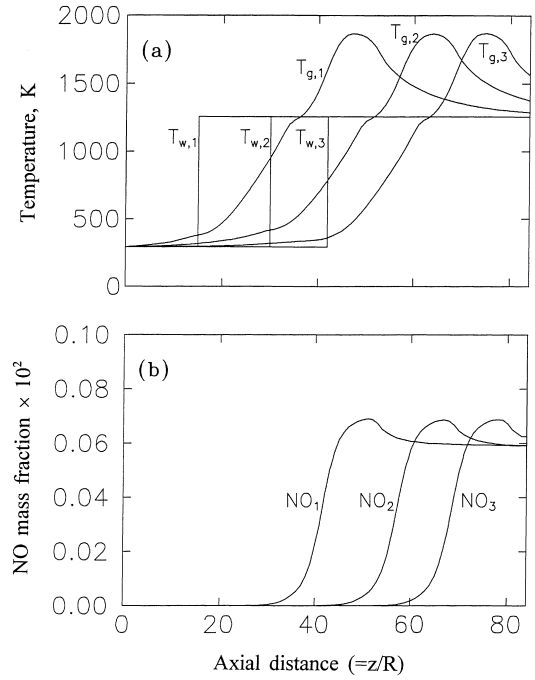

Fig. 10. The effect of the flame axial location on the gas temperature (T_g) and NO production distributions, for prescribed wall temperature (T_w) distributions (subscripts 1, 2, and 3 refer to the three flame locations).

T=1255 K from there to the combustor outlet. It was found that the axial distributions of NO were insensitive to flame location as long as sufficient time was provided for NO conversion to N_2 by the reaction with NH_3 (Fig. 10). The delayed production of NH_3 from HCN (as seen in Fig. 9(b)), causes also a corresponding delay in the destruction of NO, so that if the flame is located too close to the combustor outlet the residence time of the hot gases is inadequate for reducing the NO to its minimal values which occur at equilibrium for this combustor configuration. Indeed, Fig. 10 shows that phenomenon for the case of z=42.

Larger combustor wall emittance was found by the authors [8] to move the flame front in the upstream direction, and its effect on NO emissions was thus investigated. As shown in Fig. 11, the NO profiles remain, however, the same for different emittances, producing the same NO concentrations at the tube exit.

In the past work by Lior, Churchill and co-workers (cf. [3–6]) on NO_x production from fluid fuel combustion in the RCSC, it was determined that the primary mechanism for the measured significant reduction in NO_x emissions was the thinning of the flame zone, which has thus shortened the residence in the high temperature zone in which NO_x can be produced. We have thus examined in this study the effect of flame thickness on the NO_x emissions and found them, as shown in Fig. 12, significant. The thickness of the flame was changed by varying the amount of excess air. When a smaller amount of excess air is supplied, the flow and particle velocities are slower and combustion is completed

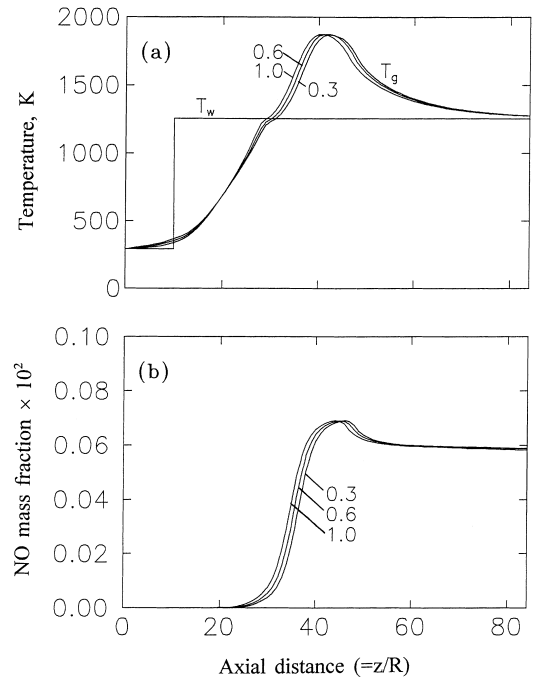

Fig. 11. The effect of the interior emittance (ε=0.3, 0.6, 1.0) of the combustor wall on the axial distributions of the, (a) gas temperature (T_g), (b) NO production, with a fixed wall temperature (T_w) distribution.

earlier and in a thinner zone. This also results in a significantly higher peak gas temperature. Smaller excess air fractions indeed reduce the residence in the flame region

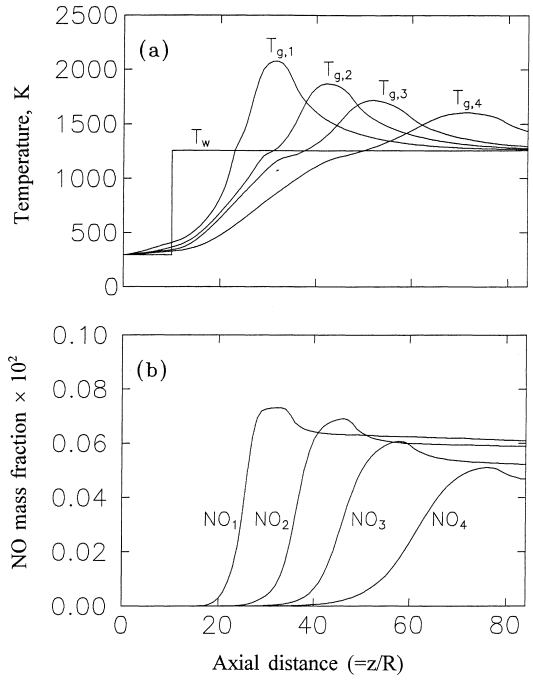

Fig. 12. The effect of flame thickness and temperature, as controlled by excess air ratio, on the axial distributions of the, (a) gas temperature (T_g), (b) NO production, with a fixed wall temperature (T_w) distribution. The subscripts 1, 2, 3, and 4 refer to excess air amounts of 50%, 100%, 150%, and 200%, respectively.

[e.g., the residence in a flame with 50% excess air (defined as 50% more air than needed for stoichiometric combustion) is about 2.5 times shorter than that in the one with 200% excess air], but they also raise the peak temperatures significantly (from 2070 K for a flame with 50% excess air down to 1060 K for the one with 200% excess air). All in all, the emitted NO *mass fraction* for the 200% excess air case (470 ppm) is 23% lower than that for 50% excess air (610 ppm). At the same time, the reaction products dilution ratio caused by the change from 50% to 200% excess is about 5, and consequently the *overall mass* of NO produced at 200% excess air is actually about 3.65-fold higher than that produced with 50% excess air. This indicates that the RCSC with its high temperature thin flame is much more effective for the reduction of NO emissions than the lower temperature combustion alternatives practised in many contemporary NO_x reduction schemes.

5. Conclusions and recommendations

A comprehensive kinetic model including 13 chemical species, and the appropriate mass transfer equations, were added to the existing conjugate heat transfer model for the radiatively/conductively-stabilized coal combustor reported in [8].

As compared with a simple three-reaction model, the radiation intensity distribution obtained by the improved model decreases substantially in the flame region, and the wall temperature increases. This is because the better kinetic model shows a lower concentration of CO_2 there due to the slow conversion of CO to CO_2, and a much lower concentration of H_2O because of its reactions with HCN and C, with a consequent decrease in the extinction coefficient of the medium. Also, the effect of a 10% deviation in the diffusion coefficients on the results was found to be negligible, indicating that the use of binary coefficients instead of those for a multi-component system may be good enough in such combustion modeling.

The NO concentration for the base case was found to peak at about 700 ppm at the axial location where the temperature peaked, and was reduced gradually towards the combustor exit, to about 600 ppm, primarily due to destruction by the NH_3 which was formed in the combustor. The results indicate that NH_3 injection into the flue gas along with the use of staged combustion or low-NO_x burner could lower NO_x emission level effectively.

The results of the sensitivity analysis show that flame location has little effect (~6%) and internal wall emittance an insignificant effect, on overall NO_x production. It was found that emitted NO *mass fractions* could be lowered by lowering the flame temperature, accomplished by increasing the excess air ratio. Nevertheless, the *overall mass* of the NO_x produced by the RCSC was still very significantly lower at the lower values of the excess air ratio which produce thinner flames of higher temperature. This points towards the conclusion that the capability of the RCSC to produce such flames has a stronger effect on overall NO_x emissions reduction than the lowering of the flame temperature practised in many contemporary NO_x reduction schemes.

6. Nomenclature

A_p	surface area of a particle, m^2
C	specific heat, J/kg K
d_p	diameter of a particle, μm
h	heat transfer coefficient, kW/m^2 K
I	total radiation intensity, kW/m^2
I_b	Planck's blackbody function, kW/m^2 μm sr
I_0	zeroth order moment of intensity, kW/m^2 μm
I_1, I_3	first order moment of intensity, kW/m^2 μm
K	overall reaction coefficient of coal, kg/N s
L	combustor tube length (=2.13 m)
k	thermal conductivity, kW/m^2 K
m	mass of a particle, kg
P_{O_2}	partial pressure of oxygen, Pa
q	heat flux, kW/m^2
q'''	heat source, kW/m^3
q_p	heat release from char oxidation (=23281 kJ/kg)
R_1	inside radius of the combustor tube (=2.54 cm)
R_2	inside radius of Fiberfrax layer (=2.86 cm)
R_3	inside radius of Fiberglas layer (=9.2 cm)

R_4 outside radius of Fiberglas layer (=15.55 cm)
r radial coordinate
T temperature, K
t time, s
u velocity, m/s
V mass of volatile matter released from coal, kg
z axial coordinate

Greek symbols

β extinction coefficient, m^{-1}
ΔH heat of pyrolysis of coal (=−418.6 kJ/kg)
ε emittance
ε_H thermal eddy diffusivity, m^2/s
κ absorption coefficient, m^{-1}
λ wavelength, μm
ρ density, kg/m^3
ω single scattering albedo ($=1-\kappa/\beta$)

Subscripts

g gas
p particle
w wall
w1 ceramic tube
w2 fiberfrax layer
w3 fiberglas layer

Acknowledgements

This work was initially partially supported by the Research Center for Advanced Energy Conversion of Nagoya University, and the authors are grateful to Prof. N. Arai for his valuable counsel. Its continuation is supported by a grant from the U.S.D.O.E. University Coal Research Program.

References

[1] D.W. Pershing, J.O.L. Wendt, 16th Int. Symp. on Combustion, The Combustion Institute, Pittsburgh, PA, 1977, 389 pp.
[2] A.N. Hayhurst, I.M. Vince, Prog. Energy Combust. Sci. 6 (1980) 35.
[3] J.W. Goepp, H. Tang, N. Lior, S.W. Churchill, AIChE J. 26 (1980) 855.
[4] S.-K. Tang, S.W. Churchill, N. Lior, 18th Int. Symp. on Combustion, The Combustion Institute, Pittsburgh, PA, 1980, 73 pp.
[5] S.-K. Tang, S.W. Churchill, N. Lior, in: R. Mahalingham, A.J. Engel (Eds.), Research Trends in Air Pollution Control: Scrubbing, Hot-Gas Clean-up, Sampling and Analysis, AIChE Symp. Ser. No. 211, vol. 77, 1981, 77 pp.
[6] S. Li, N. Lior, AIChE Paper 297b, AIChE Annual Meeting, Chicago, IL, 1990.
[7] C. Chan, N. Arai, N. Lior, S.W. Churchill, Ind. Eng. Chem. Res. 31 (1992) 681.
[8] C. Kim, N. Lior, ASME Paper No. 93-WA/HT-37, ASME, New York, 1993.
[9] M.K. Misra, Modeling of pulverized-coal flames in plug flow furnaces, Ph.D. Thesis, Department of Mechanical Engineering, Ohio State University, 1990.
[10] H. Juntgen, K.H. van Heek, Fuel 47 (1968) 103.
[11] D.B. Anthony, J.B. Howard, H.C. Hottel, H.P. Meissner, 15th Int. Symp. on Combustion, The Combustion Institute, Pittsburgh, PA, 1975, 1303 pp.
[12] H. Kobayashi, J.B. Howard, A.F. Sarofim, 16th Int. Symp. on Combustion, The Combustion Institute, Pittsburgh, PA, 1976, 411 pp.
[13] A.S. Jamaluddin, J.S. Truelove, T.F. Wall, Combust. Flame 62 (1985) 85.
[14] J.B. Howard, G.C. Williams, D.H. Fine, 14th Int. Symp. on Combustion, The Combustion Institute, Pittsburgh, PA, 1973, 975 pp.
[15] M.N. Özisik, Radiative Transfer and Interactions with Conduction and Convection, Wiley, New York, 1973.
[16] S. Tabanfar, M.F. Modest, J. Heat Transfer 109 (1987) 478.
[17] C. Kim, N. Lior, Fuel 74 (1995) 1891.
[18] C. Kim, N. Lior, N. Arai, The Symp. on Thermal Science and Engineering in Honor of Chancellor Chang-Lin Tien, 14 November 1995, University of California, Berkeley, 1995, 189 pp.
[19] L.D. Smoot, P.J. Smith, Coal Combustion and Gasification, Plenum Press, New York, 1985.
[20] W.P. Linak, J.A. McSorely, R.E. Hall, J.V. Ryan, R.K. Srivastava, J.O.L. Wendt, J.B. Mereb, Proc. Joint EPA/EPRI Symp. on Stationary Combustion NO_x Control, San Francisco, CA, 1989.
[21] N. Arai, J. Inst. Energy 67 (1994) 61.
[22] J.W. Mitchell, J.M. Tarbell, AIChE J. 28 (1982) 302.
[23] N. Arai, M. Hasatani, Y. Ninomiya, S.W. Churchill, N. Lior, 21st Int. Symp. on Combustion, The Combustion Institute, Pittsburgh, PA, 1986, 1207 pp.
[24] D.W. Pershing, J.O.L. Wendt, Ind. Eng. Chem. Process Des. Dev. 18 (1979) 60.
[25] R. Strehlow, Combustion Fundamentals, McGraw-Hill, New York, 1984.
[26] R.B. Bird, W.E. Stewart, E.N. Lightfoot, Transport Phenomena, Wiley, New York, 1960.
[27] A.M. Kanury, Introduction to Combustion Phenomena, Gordon and Breach, New York, 1975.